Materials & Design 219 (2022) 110737

Contents lists available at ScienceDirect

Materials & Design

journal homepage: www.elsevier.com/locate/matdes

Micro- and nano-environment dual-modulated anti-tendon adhesion barrier membranes

Qiang Zhang [a,1], Kui Ma [b,c,1], Chun-Hei Lam [a], Ho-Pan Bei [a], Yu Liu [a], Xing Yang [b,c,*], Xin Zhao [a,*]

[a] Department of Biomedical Engineering, The Hong Kong Polytechnic University, Hung Hom, Hong Kong, China
[b] Orthopedics and Sports Medicine Center, The Affiliated Suzhou Hospital of Nanjing Medical University, 242 Guangji Road, Suzhou 215006, China
[c] Gusu School, Nanjing Medical University, 458 Shizi Road, Suzhou 215006, China

HIGHLIGHTS

- A micro- and nano-environment dual-modulated membrane is fabricated by nano-emulsification and electrospinning techniques.
- Such membrane exhibits tailorable fiber structure, swelling, degradation, and mechanical performances.
- Such membrane can mediate on-demand siRNA delivery to prevent post-operative tendon adhesion.

GRAPHICAL ABSTRACT

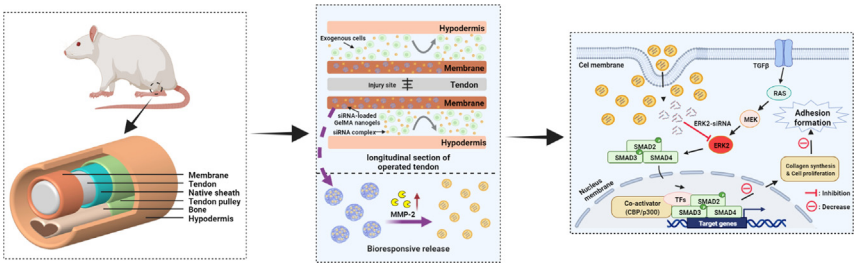

ARTICLE INFO

Article history:
Received 26 January 2022
Revised 18 April 2022
Accepted 7 May 2022
Available online 11 May 2022

Keywords:
Gene silencing
Peritendinous adhesion prevention
Micro- and nano-environment
On-demand delivery
Barrier membranes

ABSTRACT

Despite promise in preventing peritendinous adhesion, electrospun membranes face many challenges related to their complex fabrication process, untargeted/uncontrolled drug delivery and consequently low therapeutical effect. Here, a micro-and nano-environment dual-modulated barrier membrane (MNBM) with on-demand gene delivery capability is presented. Our MNBM is developed by first preparing extracellular signal-regulated kinase-2 (ERK2) siRNA-loaded gelatin methacryloyl (GelMA) nanogels via facile nano-emulsification technique, then incorporating these nanogels into poly-L-lactic acid (PLLA) fibers via simple blending electrospinning. The GelMA nanogels offer a nano-niche for ERK2-siRNA encapsulation and allow for a nano-environment controlled siRNA release by readily tuning the GelMA concentrations during nano-emulsification, while the resultant MNBM can mediate a micro-environment controlled siRNA delivery in response to the matrix metalloproteinase-2 (MMP-2) enriched micro-environment at the tendon repair site. Such MNBM can not only biologically orchestrate fibroblast behaviors by silencing the target gene expression, but also physically shield the tendon from extrinsic cell/tissue invasion. This study provides a proof-of-concept of anti-adhesion barrier membrane as an intelligent gene delivery system to offer a spatiotemporal and biophysical dual control over tendon recovery according to disease state and ensure long-term therapeutic efficacy. We envision such MNBM represents a promising therapeutic platform with great efficacy to achieve adhesion-free tendon repair.

* Corresponding authors at: Orthopedics and Sports Medicine Center, The Affiliated Suzhou Hospital of Nanjing Medical University, 242 Guangji Road, Suzhou 215006, China (X. Yang); Department of Biomedical Engineering, The Hong Kong Polytechnic University, Hung Hom, Hong Kong, China (X Zhao);
E-mail addresses: xingyangsz@126.com (X. Yang), xin.zhao@polyu.edu.hk (X. Zhao).
[1] These two authors contributed equally.

https://doi.org/10.1016/j.matdes.2022.110737
0264-1275/

1. Introduction

Peritendinous adhesion, which often leads to compromised tendon gliding (resisting joint movement), persistent pain, and even reoperation, remains the most severe clinical complication post-surgery [1]. Currently, the most desirable strategy for peritendinous adhesion prevention is to place a barrier between the injured tendon and the peripheral tissues, physically hindering extrinsic fibroblast infiltration. These barrier grafts include silica gel, gold foil, hydrogels and fibrous membranes [1]. Among them, electrospun fibrous membranes are the most popular since they can recapitulate both the fine structure and functions of native tendon sheath, allowing for diffusion of nutrients, wastes and cytokines through their pores to promote tendon healing, whilst acting as a protective shield to obstruct extrinsic cell/tissue ingrowth. To reinforce the curative nature of electrospun tendon sheaths, various pharmacological agents (e.g., ibuprofen or celecoxib) [2–4], growth factors [5], and genes [6,7] have been loaded into electrospun fibers to regulate the local pathological micro-environment and prevent fibroblast over-proliferation. However, most of these drug-loaded electrospun fibers have an uncontrollable drug release, which fail to comply with the therapeutic window of inherently dynamic tendon biology.

Here, we develop a micro-and nano-environment dual-modulated barrier membrane (MNBM) to mediate the local and repair-specific delivery of cargoes for post-operative tendon adhesion prevention. First, considering the remarkably elevated expression of matrix metalloproteinases (MMPs), especially the MMP-2, during tendon healing process as well as the excellent MMP-sensitive degradation behaviors of gelatin methacryloyl (GelMA) due to the existence of specific MMP degradation sites [8–14], we design and fabricate drug-loaded GelMA nanogels using nano-emulsification technique to realize a MMP-responsive on-demand drug delivery. In addition, such nanogel platform provides a favorable nano-niche to store drug molecules and enables a nano-environment controlled drug release by altering the concentrations of precursor GelMA solution. We select small interfering RNA (siRNA) as the drug molecule to silence extracellular signal-regulated kinase-2 (ERK2) expression, since the ERK2-related signaling pathways play positive roles in the formation of peritendinous adhesion tissue during tendon healing [15,16]. The downregulation of ERK2 will decrease the downstream SMAD2/3 expression and suppress the fibroblast proliferation and collagen production, ultimately reducing tendon adhesion formation. Another reason for choosing siRNA is the relatively long-term influence of such gene silencing strategy compared with other therapeutical molecules (e.g., pharmaceutical agents or growth factors), as the integrated gene can function within cells for a long time. After obtaining the ERK2-siRNA-laden GelMA nanogels, we develop the MNBM by encapsulating these nanogels into PLLA fibers via facile blending electrospinning technique. We find this all-in-one MNBM shows tailorable fiber diameter, excellent mechanical performances, superior swelling and degradation properties, as well as micro-environment controlled siRNA release behavior. After implantation of MNBM to the tendon injury site, the elevated MMP-2 in the regional micro-environment can catalyze the biodegradation of the incorporated GelMA nanogels and expedite the ERK2-siRNA release from the MNBM. The released ERK2-siRNA will then be transfected into fibroblasts and downregulate the target gene expression to inhibit the key fibrosis signaling pathway, ultimately suppressing cell proliferation and collagen deposition and alleviating the peritendinous adhesion *in vivo* (Fig. 1 **B-D**). Altogether, our study provides a proof-of-concept of barrier membranes as an intelligent gene delivery platform to form a positive chain reaction (i.e., disease trigger-drug release-disease treatment) to match the changing tendon healing progression, offering an effective intervention in fibrosis tissue formation by micro- and nano-environment dual-modulation while diminishing the off-target effect of the drugs. We envision that our MNBM will advance the development of high-performance barrier grafts towards tendon tissue engineering and find extensive applications for other diseases with locally elevated MMP expressions such as diabetes mellitus-associated skin impairment, osteoarthritis, and solid tumor, etc.

2. Experimental section

2.1. Preparation of siRNA-laden GelMA nanogels

First, methacrylated gelatin (GelMA) was synthesized according to our previously reported methods [17,18]. Briefly, 15.0 g gelatin (Type A, Sigma-Aldrich, Hong Kong) was dissolved in 150 mL phosphate buffered saline (PBS, HyClone™) at 60 °C under vigorous stirring, and then 16 mL methacrylic anhydride (Sigma-Aldrich, Hong Kong) was added slowly to react with the gelatin at 50 °C for 3 h. The mixture was then dialyzed (MWCO 8,000–14,000, OAMAY) to remove any byproduct and unreacted methacrylic anhydride.

To prepare siRNA-laden GelMA nanogels, the siRNA transfection mixture was obtained by mixing the ERK2-siRNA (10 nM) with a commercial cationic polymeric transfection reagent, jetPRIME® siRNA Transfection (Polyplus-transfection® company, Hong Kong), in distilled water at room temperature for 8 min following the manufacturer's instructions. siRNA was purchased from GenePharma Co., Ltd., Shanghai, China, and their sequences were shown as follow: ERK2-siRNA: 5′- CACCAGACCUACUGUCAAATT-3′ (sense), 5′- UUUGACAGUAGGUCUGGUGTT-3′ (antisense); negative control (NC): 5′-UUCUCCGAACGUGUCACGUTTACGUGACACGUUCG GAGAATT-3′. Cy3 dye was introduced to the 5-end of the antisense strand to enable fluorescence observation. Afterwards, GelMA nanogels containing the siRNA transfection mixture were prepared by water-in-oil (W/O) nano-emulsification technique [19,20]. Briefly, the GelMA aqueous solutions (5%, 10%, and 20%, w/w) containing 0.5% (w/v) photo-initiator lithium phenyl-2,4,6-trimethyl benzoylphosphinate (LAP, Sigma-Aldrich, Hong Kong) were prepared by dissolving the as-synthesized GelMA and LAP in 3 mL PBS (pH 7.4) followed by addition of 500 μL as-prepared transfection mixture. Once thoroughly mixed, the siRNA/GelMA aqueous solution was dropwise added into n-octane oil phase (Macklin Reagent, China) containing surfactant mixtures (Span 80 (Sigma-Aldrich, Hong Kong): Tween 80 (Sigma-Aldrich, Hong Kong) at a weight ratio of 2:3. The weight ratio of water phase: oil phase: surfactants was fixed at 1:4:1. The resultant mixture was then subjected to stirring by mechanical homogenizer (Ultra-Turrax T25, IKA) for 10 min at speed of 8000 rpm/min to get crude emulsion. Finally, the fine and homogeneous emulsion was obtained by ultrasonic processor (Scientz® JY96-IIN, Ningbo, China) under 400 W for 1 min. The whole process was performed at 4 °C in the sealed ice bath out of light. Photo-crosslinking was carried out by exposure of the emulsion to ultraviolet (UV) light (OmniCure® Series 1500 lamp, Excelitas Technologies Corporation, USA) at density of 10 W/cm^2, light source of 250–450 nm, and irradiation time of 10 min. The resulting GelMA nanogels were finally added with tetrahydrofuran (THF, Sigma-Aldrich, Hong Kong) and centrifuged to remove the organic phase and surfactant. Here, we developed three groups of siRNA-containing GelMA nanogels including G1/S, G2/S, and G3/S, which were prepared with GelMA concentrations of 5, 10 and 20 wt%, respectively.

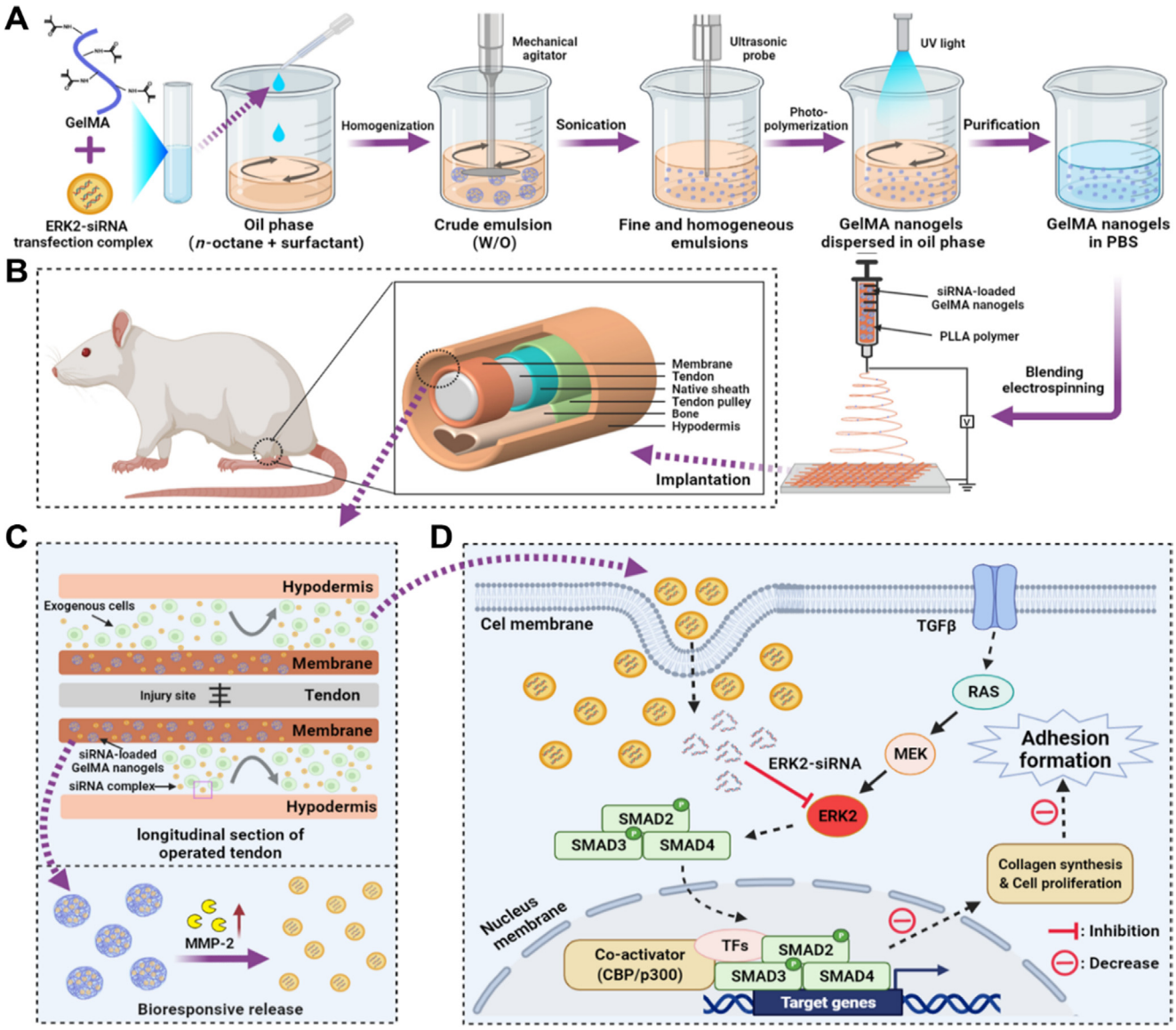

Fig. 1. Schematic illustration showing the development of MNBM for prevention of tendon adhesion. (A) The preparation process of siRNA-laden GelMA nanogels via nano-emulsification technique and subsequent composite fibrous membranes via blending electrospinning. (B) The resultant MNBM is implanted to the tendon injury site, serving (C) as a physical barrier to prevent exogenous cell invasion while as a drug reservoir to release therapeutical ERK2-siRNA molecules triggered by the elevated MMP-2 in the tendon healing micro-environment. (D) The released ERK2-siRNA complexes downregulate the expression levels of ERK2 and its downstream signaling molecules and suppress fibroblast adhesion/proliferation and collagen deposition, reducing the scar tissue formation. Figure created with BioRender.com.

2.2. Characterization of siRNA-laden GelMA nanogels

2.2.1. Morphology characterization

Particle size was measured by dynamic light scattering (DLS) (Malvern Zetasizer Nano ZS; Malvern, UK). The morphology of ERK2-siRNA transfection mixture and GelMA nanogels was analyzed by transmission electron microscopy (TEM) (Tecnai G220 S-TWINScanning, FEI, OR, USA).

2.2.2. In vitro cell transfection

Fibroblasts (murine cell line, NIH-3T3 cells, ATCC® CRL-1658™) were transfected with ERK2-siRNA mixture according to the manufacturer's protocols. NIH-3T3 cells were cultured using Dulbecco's Modified Eagle Medium (DMEM, Gibco, Hong Kong) supplemented with 10 vol% fetal bovine serum (FBS; Gibco, Hong Kong) and 1 vol % penicillin/streptomycin (PS; Gibco, Hong Kong) in a 5% CO_2 incubator at 37 °C. Cy3-labeled ERK2-siRNA was used to observe the siRNA localization within cells, while normal culture medium was used as the blank control.

2.2.3. In vitro siRNA release from GelMA nanogels

To assess the siRNA release profile from the GelMA nanogels, 5 mg freeze-dried siRNA-containing GelMA nanogels was incubated in 1 mL PBS with different concentrations of MMP-2 (Gibco, Hong Kong) (0, 0.2, 2 U/mL) for 72 h [21,22]. At given time interval, 0.1 mL of supernatant was collected for analysis followed by supplement with same amount of PBS (0.1 mL). The siRNA concentration was analyzed using a Quant-iT™ RiboGreen RNA Assay Kit (Invitrogen, Thermo Fisher Scientific, Inc. Hong Kong) and quantified by microplate reader (BioTek, US) at excitation wavelength of 485 nm and emission wavelength of 520 nm. Besides, the siRNA loading efficiency of GelMA nanogels was evaluated following previous protocols [22,23]. Briefly, 2 mg siRNA-containing GelMA nanogels were dispersed in 1 mL of PBS added with 40 U/mL

MMP-2, and incubated at 37 °C overnight to facilitate the extraction of siRNA from GelMA nanogels. Subsequently, after centrifugation for 30 min at 13,000 g, the supernatant was collected and analyzed by a Quant-iT™ RiboGreen RNA Assay Kit as described above. Each sample was measured in triplicate. The siRNA loading efficiency was calculated following the below equation:

$$\text{Loading efficiency} = \frac{\text{Total siRNA released} + \text{Total siRNA extracted}}{\text{Theoretical total siRNA loading}} \times 100\%$$

2.2.4. In vitro intracellular uptake of siRNA

The intracellular uptake of siRNA released from GelMA nanogels was assessed by co-culture of NIH/3T3 with the leaching solutions, which were prepared by incubating siRNA-containing GelMA nanogels in culture medium containing MMP-2 (2 U/mL) for 24 h at 37 °C. Then, after seeding NIH/3T3 in the 24-well plates at a density of 2×10^4 cells/mL and culturing overnight, 1 mL extract was added to the 24-well plate and continuously incubated for 1 day. After staining the cytoskeleton and cell nucleus by phalloidin staining (Thermo Fisher, Hong Kong) and 4′,6-diamidino-2-pheny lindole (DAPI) staining (Thermo Fisher, Hong Kong), respectively [24]. samples were observed using a fluorescence microscope (Nikon, Japan). Here, normal culture medium (control) was used as the blank control, while GelMA nanogels without loading siRNA (G2) or loading with Cy3-labeled negative control-siRNA (G2/NC) as the negative controls. The average cell area was evaluated based on four representative images via Image J software following our previous protocol [24].

2.3. Preparation of GelMA nanogel-embedded electrospun fibrous membranes

The electrospun fibrous membranes incorporated with siRNA-containing GelMA nanogels were fabricated using blending electrospinning. Briefly, PLLA (Mw = 10 kDa, Jinan Daigang Co., Jinan, China) was dissolved in HFIP (20%, w/v, Aladdin, Shanghai, China) and then different amounts of siRNA-containing GelMA nanogels were dispersed evenly into PLLA electrospun solution by constant stirring prior to electrospinning process. Here, five groups of electrospun fibrous membranes were developed including Pure PLLA, 1 %G2/S/PLLA, 5 %G2/S/PLLA, 10 %G2/S/PLLA, 20 %G2/S/PLLA, which were prepared at mass ratios of siRNA-containing GelMA nanogels (G2/S) to PLLA set at 0, 1%, 5%, 10%, and 20% (w/w). The electrospinning parameters were 15 kV for applied voltage, 1 mL/h for pump rate, and 10 cm for distance between syringe and collector.

2.4. Physical characterization of electrospun membranes

2.4.1. siRNA distribution and morphology

The siRNA distribution and fibrous morphology of electrospun membranes were examined by monitoring the electrospun membranes containing Cy3-labeled siRNA under a fluorescence microscope (Nikon, Japan).

2.4.2. Swelling, degradation and mechanical properties

The swelling properties of GelMA nanogel-embedded fibrous membranes were evaluated following our previous protocol [17]. Briefly, samples were disinfected and lyophilized and their initial (dry) weight was measured (S_0). The specimen membranes (1 cm diameter) of each group were then put into 2 mL of PBS and incubated at 37 °C. At specific intervals (0, 2, 4, 6, 12, 24, 48, 96 h), the specimen membranes were taken out and weighed (S_1) after wiping the residual water on the membranes' surface using filter papers. The swelling percentage (SP) was calculated by the equation: $SP = S_1/S_0 \times 100\%$. In addition, the morphology changes of membranes before and after swelling in PBS for 3 days were investigated by scanning electron microscopy (SEM) (Tescan VEGA3, Czech Republic). Before SEM observation, the electrospun membranes were coated with gold in a sputter coater.

The degradation profile of electrospun fibrous membranes was evaluated by immersing samples in PBS at 37 °C [25]. Briefly, initial weight (W_0) of membrane samples (circular specimens with 1 cm diameter and 1 mm thickness) was recorded. Then, samples were immersed in 2 mL of PBS containing different concentrations of MMP-2 (0, 0.2, 2, 10 U/mL), and incubated at 37 °C for 14 days with shaking at 100 rpm. The MMP-2-containing PBS solution was refreshed every 2–3 days to ensure the enzymatic activity. At the pre-determined time points (0, 2, 4, 12 h, 1, 2, 4, 7 and 14 days), samples were collected, rinsed with deionized water, freeze-dried for 24 h, and weighed to determine the residual mass (W_t). The degradation percentage of membranes was determined according to the equation: Degradation percentage (%) = $(W_0\text{-}W_t)/W_0 \times 100\%$.

The mechanical performances of electrospun fibrous membranes were assessed by tensile test using a mechanical tester (Instron, US) [24]. Briefly, the fibrous membranes were cut into 50 mm × 10 mm rectangular samples followed by measuring the thickness of each sample by a micrometer (Syntek, China). Then, samples (n = 4) were fixed to the instrument by pneumatic clamps and stretched longitudinally at a speed of 5 mm/min until failure to obtain the stress-stain curve.

2.4.3. In vitro siRNA release from electrospun membranes

siRNA-containing electrospun membranes (about 10 mg) were incubated in 1 mL PBS added with different concentrations of MMP-2 (0, 0.2, 2 and 10 U/mL). At the pre-determined time points (0, 2, 4, 8, 12, 24 h, 2, 4, and 7 days), 0.2 mL supernatant was harvested, and same amount of fresh PBS solution was supplemented. the siRNA concentration in the supernatant was detected via Quant-iT™ RiboGreen RNA Assay Kit. The residual siRNA inside the fibers after 7-day release study was determined by dissolving the samples in 1 mL chloroform followed by addition of 200 μL TE buffer to extract the siRNA-containing GelMA nanogels. Then, the aqueous phase was collected, added with 400 μL MMP-2-containing PBS solution (40 U/mL) and finally measured via Quant-iT™ RiboGreen RNA Assay Kit.

2.5. In vitro biological characterization of electrospun membranes

2.5.1. Cell viability assay

The effect of electrospun membranes on cell viability was evaluated by live/dead staining. Briefly, we first prepared the leaching solution of different fibrous membranes by immersing the samples in the complete culture medium with or without the addition of MMP-2 (2 U/mL) for 24 h at 37 °C. Then, after seeding NIH/3T3 in 24-well plates at a density of 2×10^4 cells/mL and incubating overnight, the medium was aspirated, and 1 mL extract of different samples was added to each well. After 3-day culture, cells from different groups were stained using Live/Dead assay kit (Thermo Fisher, Hong Kong) according to the manufacturer's protocol, and observed using a fluorescence microscope (Nikon, Japan). The results were expressed as the ratio of the dead cells to live cells processed by ImageJ software [24].

2.5.2. Immunofluorescence studies

To observe the cell morphology and visualize ERK expression, immunofluorescence staining was performed. Briefly, after co-culture for 3 days, cells in the well plates were fixed by 4% paraformaldehyde (Sigma-Aldrich, Hong Kong) for 20 min, and incubated in 0.1% Triton X-100 (Sigma-Aldrich, Hong Kong) for 20 min followed by addition of 1% Bull Serum Albumin (BSA) (Sigma-Aldrich, Hong Kong) to block the non-specific protein. Then, the intracellular filament F-actin, ERK, and cell nuclei were

stained with phalloidin (Thermo Fisher, Hong Kong), anti-p-ERK1/2 (Abcam, UK), and DAPI (Thermo Fisher, Hong Kong), respectively, following the manufacturer's protocols [26]. Finally, the samples were photographed with a fluorescence microscope (Nikon, Japan). The mean cell fluorescence intensity was analyzed using ImageJ software.

2.5.3. Cell proliferation evaluation

The cell proliferation of NIH/3T3 after treatment with different fibrous membranes for 1 and 3 days was revealed by Cell Counting Kit-8 (CCK8) analysis (Beyotime Biotechnology, China). The cells cultured in normal culture medium was used as the control group. In brief, CCK-8 solution was added to each well at a volume of 10% of the culture medium. After 4-h treatment, the sample absorbance at 450 nm was detected by a microplate reader (BioTek, US). The average absorbance value of each group was normalized to indicate the cell proliferation.

2.5.4. Bioactivity assessment of delivered siRNA

Quantitative real-time polymerase chain reaction (qRT-PCR) was performed to assess the bioactivity of the released ERK2-siRNA by measuring the expression of targeted ERK2 and its downstream signalling molecules (collagen type I (Col-1) and collagen type III (Col-3)) by NIH/3T3 cells [17,24]. In brief, after 3-day incubation, the cells were harvested, and Total RNA Kit (Omega, Hong Kong) was used to extract the total RNA from NIH/3T3 cells. Then, PrimeScript RT Master Mix Kit (Takarabio, Hong Kong) was used to reverse-transcribe RNA to complementary DNA, followed by PCR detection using the Real-Time PCR Detection System with TB Green Premix Ex Taq Kit (Takarabio, Hong Kong). Glyceraldehyde-3-phosphate dehydrogenase (GAPDH) was used as an internal control for normalization. The primer sequences were shown in the **Table S1**.

2.6. In vivo anti-tendon adhesion evaluation

2.6.1. Establishment of rat achilles adhesion model

All animal experimental protocols were approved by the Ethics Committee of the Hong Kong Polytechnic University (18-19/7-BME-R-HMRF) and the Affiliated Suzhou Hospital of Nanjing Medical University. A total of 48 male SD rats (6–8 weeks, weighting between 200 g and 300 g) were randomly divided into four groups including control (no treatment), positive control (using the Surgi-Wrap, a commercial biodegradable anti-adhesion barrier film, as the wounding dressing), 10 %G2/PLLA, and 10 %G2/S/PLLA. The rats were anesthetized by intravenous injection of 3% pentobarbital sodium (30 mg/kg) and fixed in the prone position, followed by shaving and disinfecting their hind foot. Then, the tendon was transected through a posterior midline skin incision 5 mm away from the talocalcaneal tuberosity, and repaired using a modified Kessler tendon suture technique. Finally, membrane samples (1×2 cm^2) from each group were wrapped around the surgical site before skin wound was closed with a 4-0 silk suture.

2.6.2. Macroscopic evaluation

After surgery for 21 days, the operated limbs were retrieved for gross assessment of any inflammation or ulcer. Then, the repair sites were opened to macroscopically evaluate the severity of tendon adhesion using a semiquantitative scoring system [27]. Score 1 represents nearly no adhesion; Score 2 represents few fibrous tissues were attached onto the surface of surgical sites, which can be readily separated by blunt dissection; Score 3 represents $\leq$50% of area around the tendon was covered with the fibrous tissues, which could be separated by blunt rather than sharp dissection; Score 4 represents 51–97.5% of area around the tendon was covered with the fibrous tissues, which could only be separated by sharp dissection; Score 5 represents >97.5% of area around the tendon was covered with the fibrous tissues, which could only be separated by sharp dissection. The specimens were evaluated in parallel by two pathologists without their knowledge.

2.6.3. Histological and immunohistochemical examination

The repaired sites of tendons were retrieved and fixed in 10% formalin for 24 h. Then, specimens were washed, dehydrated with a graded series of ethanol, and embedded in paraffin wax followed by cutting into sections of 5 μm thickness using a rotary microtome and staining with hematoxylin-eosin (H&E) and Masson's trichrome. The light microscopy was used to observe the sections of histologic adhesion area. The histological adhesion evaluation was performed based on the H&E and Masson's trichrome staining images following the previously published protocols [28–30].

Expressions of Col-1 and Col-3 in the peritendinous adhesion tissues were evaluated by immunohistochemical staining. Briefly, the sections were dewaxed by xylene and hydrated in gradient alcohol. Then, the sections were placed in a citrate buffer solution (pH = 6.0) and heated to 60 °C for 20 min to recover the antigen. Then, endogenous peroxidase activity was neutralized using 3% hydrogen peroxide, and unspecific antigen cross-reaction was blocked using goat serum (1:100 diluted, Bioshark, China). Subsequently, samples were incubated with primary antibody against Col-1 or Col-3 (1:200, Abcam, UK) for 12 h at 4 °C, followed by rinse with PBS and immersion in 3,3′-diaminobenzidine (DAB) solution (Dako, Germany) for stanning development. The relative optical density of Col-1 and Col-3 was quantified by ImageJ software.

2.6.4. Biomechanical testing

The harvested tendon specimens were fixed onto the clamps of a mechanical tester (Instron 5548, US) following the published protocols [5]. Then, the maximal breaking force of samples was evaluated by pulling at a speed of 20 mm/min with a preload of 1 N until the tendons were completely ruptured.

2.6.5. Western blot analysis

The protein expressions of p-ERK1/2, p-SMAD3, Col-1, Col-3, and β-actin were evaluated by western blotting following the previous protocols [17,31]. The primary antibodies against p-ERK1/2, p-SMAD3, Col-1, Col-3, and β-actin (1:1000 dilution; Abcam, UK) and secondary antibody (1: 3000 dilution; Abcam, UK) were used. The immunoreactive bands were visualized using an enhanced chemiluminescence reagent (Amersham Biosciences, USA), and their optical intensity was further quantified using Photoshop software (Adobe, USA).

2.7. Statistical analysis

All measurements were conducted in quadruplicate if not specified. The quantitative data were presented as the mean ± standard deviation (SD). The between-group differences were assessed using one-way analysis of variance (ANOVA) followed by Tukey's multiple comparison tests (SPSS Statistics 17.0., IBM Corp., USA). A p-value less than 0.05 was considered statistically significant.

3. Results and discussion

3.1. Characteristics of siRNA-laden GelMA nanogels

In this study, we used GelMA as the basis to develop microenvironment-sensitive siRNA-encapsulated vehicles not only due to its MMP-responsive degradation profile and excellent biocompatibility, but also its low-cost production. We synthesized GelMA by chemically grafting methacrylic anhydride onto gelatin. The

methacrylation of gelatin was confirmed by ^{1}H-nuclear magnetic resonance (^{1}H NMR) spectrum, in which a distinctive double peak (vinyl proton signal) appeared around 5.5 ppm while the lysine signal at 2.9 ppm decreased (**Fig. S1**). Then, ERK2-siRNA transfection complex was prepared and exhibited a spherical structure with uniform particle size (**Fig. S2A and B**). *In vitro* cell transfection study further demonstrated such siRNA transfection complex could transfect cells and exert gene silencing effectively (**Fig. S2C**).

Subsequently, we developed siRNA-laden GelMA nanogels via nano-emulsification technique, during which siRNA-containing GelMA aqueous solution served as the water phase and *n*-octane as the oil phase. After photocrosslinking under UV irradiation, we obtained a fine and stable emulsion that was transparent without phase separation (**Fig. S2D**). To assess the particle size distribution and morphology of the prepared siRNA-laden GelMA nanogels, we then performed DLS and TEM as size characterization. As shown in Fig. 2**A**, GelMA nanogels for all groups showed homogeneous distribution, and their average diameters increased with the GelMA concentrations adopted to fabricate the nanogels. TEM results were in accordance with DLS analysis, demonstrating that the siRNA-laden GelMA nanogels displayed uniform spherical shape with their diameters increasing with GelMA concentrations (Fig. 2**A**). Next, to demonstrate whether such GelMA nanogels could encapsulate the siRNA, we used a fluorescence microscope to observe the fluorescence signal of Cy3-labeled siRNA in the nanogels (Fig. 2**B**). Compared with pure GelMA group, there were many

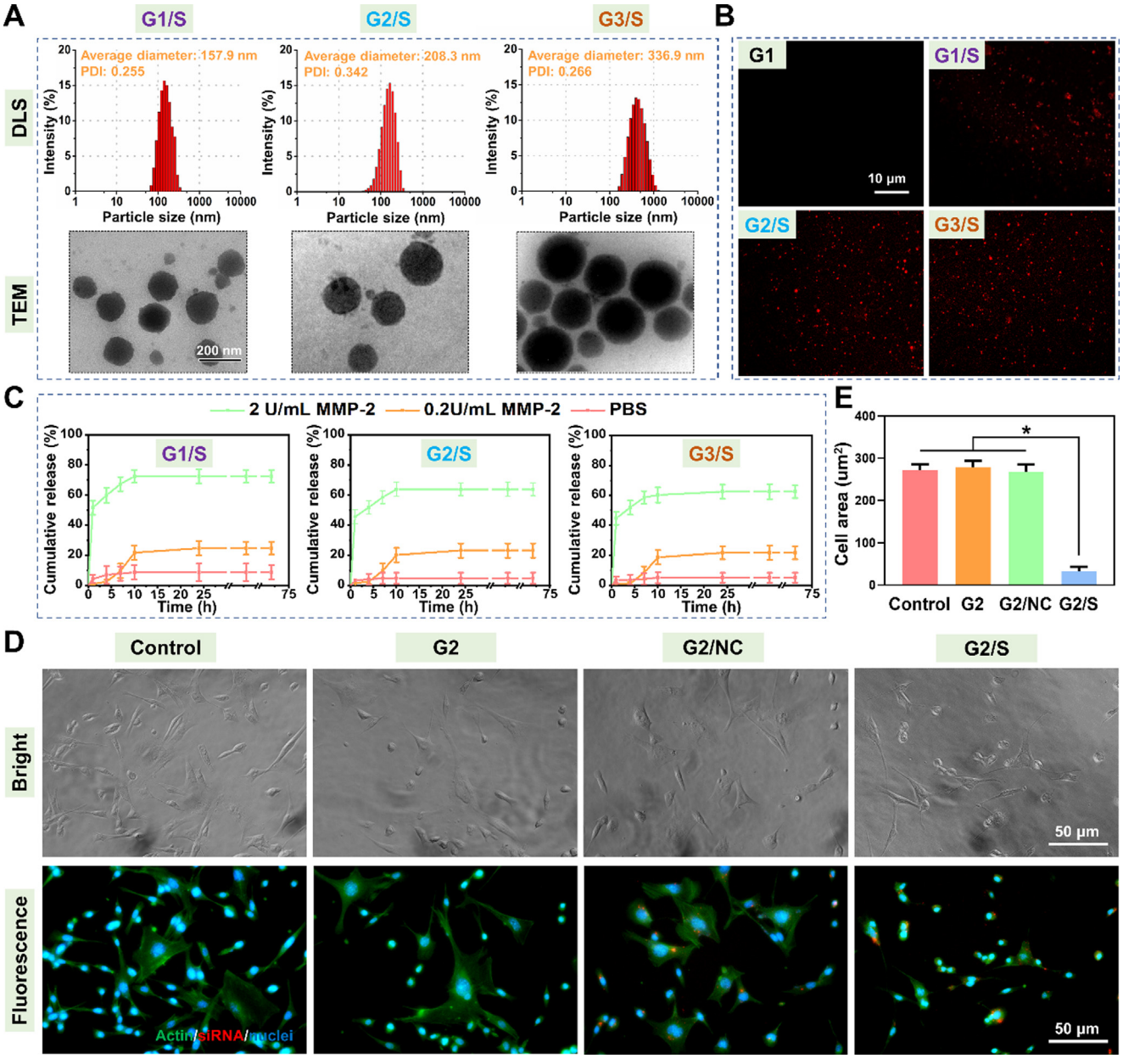

Fig. 2. Morphology and characterization of siRNA-laden GelMA nanogels. (A) DLS analysis and TEM images, and (B) fluorescence observation of different GelMA nanogels. (C) *In vitro* ERK2-siRNA cumulative release from different GelMA nanogels incubated in PBS with different concentrations of MMP-2 (0, 0.2, and 2 U/mL). G1/S, G2/S and G3/S represent the siRNA-laden GelMA nanogels prepared with GelMA concentrations of 5, 10 and 20 wt%, respectively. (D) Intracellular uptake of ERK2-siRNA determined by immunofluorescence staining. F-actin and nuclei were stained by phalloidin (green) and DAPI (blue), respectively. ERK2-siRNA or negative control-siRNA (NC) was labeled by 5′-Cy3 (red). (E) Quantitative analysis of the cell area after treatment with different material formulations for 1 day. Data were expressed as mean ± SD and evaluated by one-way ANOVA followed by Tukey's multiple comparison tests (n = 4, * represented $p < 0.05$).

scattered red fluorescence signals in the G1/S, G2/S and G3/S groups, which demonstrated the successful encapsulation of siRNA into GelMA nanogels. Besides, we found these nanogels were dispersed homogeneously without any substantial agglomeration, which would be beneficial for further application. Altogether, these results established the feasibility of using nano-emulsification strategy to prepare the siRNA-laden GelMA nanogels.

We then evaluated the siRNA cumulative release profile from different GelMA nanogels incubated in MMP2-containing PBS (0, 0.2, 2 U/mL) (Fig. 2**C**). In PBS solution without addition of MMP-2, we found a small amount of siRNA release into the solution in the G1/S, G2/S and G3/S groups, which could be attributed to the diffusion of siRNA complexes located onto the outer surface of the GelMA nanogels. However, the cumulative release rapidly reached a plateau. This might be in large part due to the electrostatic interaction between the GelMA nanogels (positive charge) and the siRNA (negative charge) that limited the siRNA desorption and diffusion, aside from the physical barrier retention by GelMA. Notably, these GelMA nanogels showed increased siRNA release rates with higher MMP-2 concentrations thanks to the presence of specific MMP degradation sites [14]. The cumulative siRNA release amount for all groups exceeded 50% within the first 4 h upon incubation in 2 U/mL MMP-2 solution. More importantly, we found that the higher GelMA concentrations adopted to prepare nanogels, the lower the siRNA release rate, indicating the siRNA release kinetics from the GelMA-formed nano-environment could be readily modulated by regulating the GelMA concentration. Such phenomenon could be attributed to the increased crosslinking density at higher GelMA concentration. The siRNA loading efficiency of our proposed nanogel platform was further investigated. The experimental loading efficiencies for G1/S, G2/S and G3/S were found 66.84 ± 4.69%, 64.97 ± 3.41% and 48.73 ± 5.32%, respectively. The remarkably reduced loading efficiency for G3/S might be due to the increment of GelMA solution viscosity that could lead to the loss of siRNA during the nano-emulsification process. Altogether, such GelMA nanogel platform could offer a suitable nanoniche for controllable and MMP-triggered siRNA delivery. Given the suitable particle size, appropriate siRNA release pattern, and relatively high loading efficiency, G2/S was selected in the following studies.

To assess the transfection efficacy of siRNA released from GelMA nanogels, we evaluated the *in vitro* intracellular siRNA uptake and the corresponding change in cell morphology. As illustrated in the Fig. 2**D**, compared with the control and G2 groups, Cy3-labeled siRNA (red) could be observed in the G2/NC and G2/S groups, suggesting that the loaded siRNA could be released from GelMA nanogels and then transfected into NIH/3T3 cells. More importantly, although no significant difference in average cell spreading area was found among control, G2 and G2/NC groups, the G2/S showed a remarkably lower cell spreading area (Fig. 2**D and E**). This could be ascribed to the blocking of ERK2-associated signalling pathway by ERK2-siRNA, which ultimately reduced collagen deposition and fibroblast adhesion [15]. These results collectively demonstrated that our prepared GelMA nanogels could retain the ERK2-siRNA's biofunction while realizing MMP-sensitive on-demand release, showing huge potential as a smart siRNA carrier.

3.2. Morphology, swelling and mechanical performances of MNBM

We prepared MNBM by simple co-electrospinning of a mixed precursor containing PLLA and GelMA nanogels. To evaluate whether the GelMA nanogels were encapsulated in the PLLA fibers, we examined the distribution of Cy3-labeled siRNA-laden GelMA nanogels within the fibers by fluorescence observation. As shown in Fig. 3**A**, strong red fluorescent signals were detected in the GelMA nanogel-containing groups, but not in the pristine PLLA. Importantly, the fluorescence intensity was remarkably enhanced with the increase of the GelMA nanogel content (Fig. 3**C**), suggesting that the siRNA loading amount could easily be controlled by changing the incorporated nanogel content. These results confirmed the successful fabrication of the composite electrospun membranes. Next, we investigated the surface morphology of the fabricated MNBM via SEM (Fig. 3**B**). Such composite electrospun membranes exhibited an ECM-mimicking nanofibrous structure with a randomly interconnected network, uniform size, and smooth surface. The average fiber diameter decreased with increase of the embedded GelMA nanogel contents, which was in the range of 0.47 ± 0.19 μm to 0.83 ± 0.11 μm (Fig. 3**D**). Besides, we observed the nanoscale porosity of such electrospun fibers, which could facilitate the transportation of nutrients and wastes to promote intrinsic healing while limiting exogenous cell invasion to prevent extrinsic healing (often caused the adhesion formation). To evaluate the hygroscopicity of the MNBM, we assessed their swelling ratio. Our results indicated that the swelling properties were dependent on the embedded GelMA nanogel content, albeit with limited influences (Fig. 3**E**). Among these groups, 20 %G2/S/PLLA exhibited the most distinct water sorption (absorbed water equivalent to only ~7% of its dry weight after immersion in PBS for 6 h). SEM further attested the significant morphology changes for GelMA nanogel-containing electrospun membranes before and after swelling (Fig. 3**B and D**). The high swelling ratio is beneficial for siRNA release from the hydrophobic PLLA fibers.

We then proceeded to the assessment of the MNBM's mechanical properties by tensile stress-stain measurements. Ideally, a good barrier scaffold should possess robust mechanical strength to facilitate the surgical operation process and maintain the structural integrity during long-term *in vivo* implantation while remaining pliable to avoid accidental damage to surrounding tissues. Our results demonstrated that the mechanical properties of MNBM significantly decreased after increasing the GelMA nanogel content (Fig. 3**F, 3G and 3H**). Amongst these groups, the 20 %G2/S/PLLA exhibited the lowest mechanical performances with a tensile modulus of 20.49 ± 5.55 MPa and a fracture strain of 33.91 ± 3.90%. Such significantly reduced mechanical properties might be due to the low interfacial interaction between PLLA and GelMA nanogels, as well as the nanogel aggregation upon increase of their content in the PLLA fibers. However, even for the 20 %G2/S/PLLA group, its mechanical properties could still resist external forces without graft failure, meeting the requirement of practical application. Combined with the results of swelling and mechanical tests, we selected the 10 %G2/S/PLLA for the following experiments due to its relatively appropriate swelling ratio and high mechanical performances.

3.3. In vitro enzyme-triggered siRNA release and degradation profile

In our designed barrier membranes, we aim to regulate cell behaviors in response to the elevated expression of MMP-2 in peritendinous tissue. Thus, we evaluated the siRNA release from MNBM by incubating samples in PBS containing different concentrations of MMP-2. It was observed that siRNA could be slowly released from the fibrous membranes immersed in the pure PBS, with cumulative release percentage reaching plateau (16.83 ± 3.76%) after 24-h incubation (Fig. 3**I**). Such phenomenon might be attributed to the swelling process of the incorporated GelMA nanogels, in which a small amount of siRNA could diffuse outside when water infiltrated the GelMA network. Of note, the addition of MMP-2 significantly promoted the siRNA release from the fibrous membranes; the higher concentration of MMP-2, the faster release rate and the higher cumulative release percentage of siRNA. Given the extremely slow biodegradation rate of PLLA

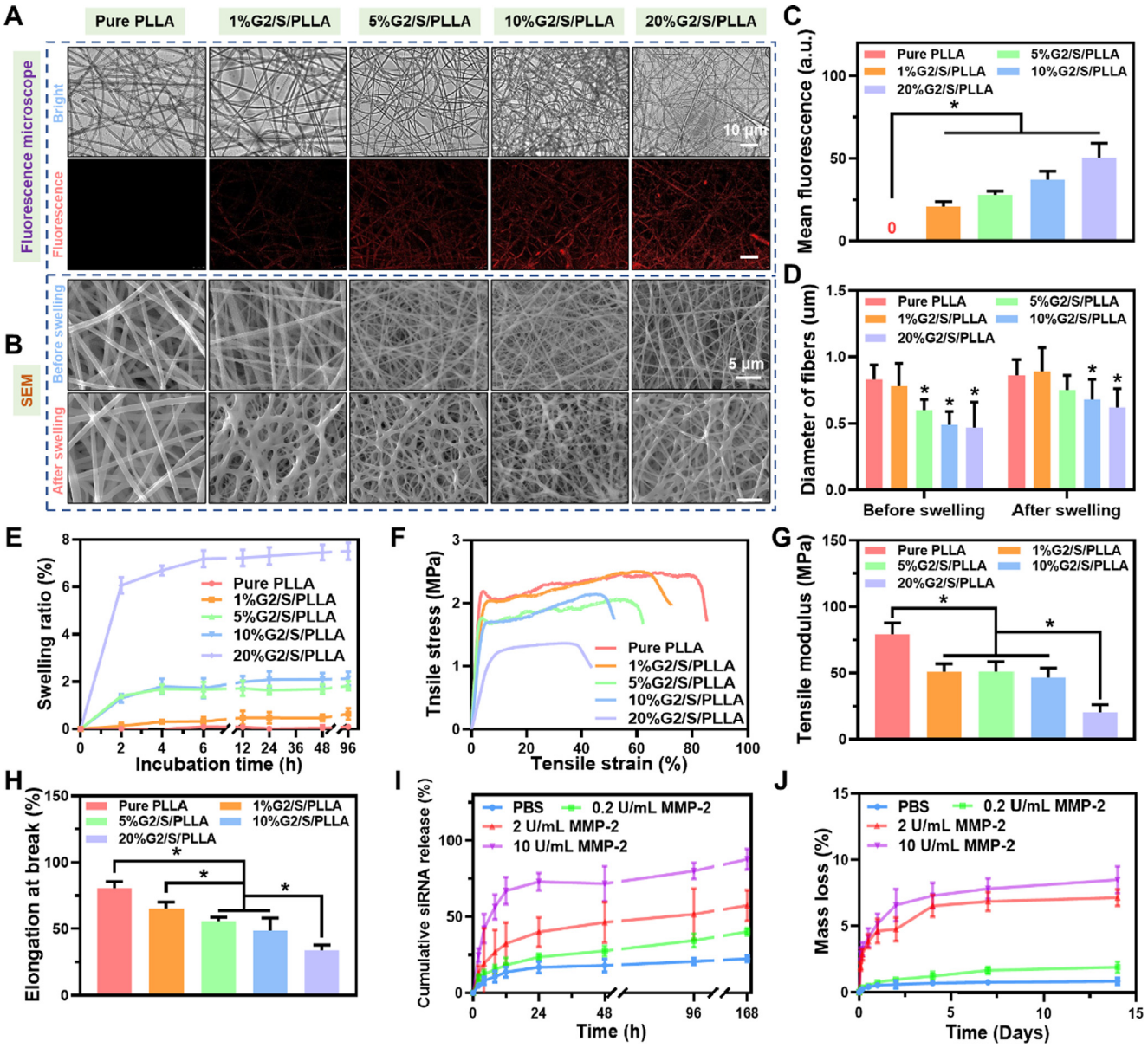

Fig. 3. Morphology and characterization of MNBM. (A) Fluorescence observation and (C) mean fluorescence intensity of different PLLA fibrous membranes. Red fluorescence indicated the Cy3-labeled siRNA-laden GelMA nanogels embedded in the PLLA fibers. (B) Representative SEM images and (D) fiber diameter distribution of the prepared electrospun membranes before and after swelling in PBS for 3 days. (E) Swelling ratio of different electrospun membranes after incubation in PBS for 96 h. (F) Representative stress-strain curves of tensile test of different PLLA membranes. (G) Tensile modulus and (H) elongation at break of the prepared electrospun membranes calculated from the tensile stress-strain curves. (I) *In vitro* ERK2-siRNA release profile and (J) mass loss of 10 %G2/S/PLLA when incubated in PBS containing different concentrations of MMP-2 (0, 0.2, 2 and 10 U/mL). 1 %G2/S/PLLA, 5 %G2/S/PLLA, 10 %G2/S/PLLA and 20 %G2/S/PLLA referred to the MMP-2 responsive electrospun membranes prepared with mass ratios of siRNA-containing GelMA nanogels (G2/S) to PLLA at 1%, 5%, 10%, and 20% (w/w), respectively. Data were expressed as mean ± SD and evaluated by one-way ANOVA followed by Tukey's multiple comparison tests (n = 4, * represented $p < 0.05$).

[32,33] and the presence of abundant MMP degradation sites in GelMA [12,13], we speculated such enzyme-triggered siRNA release profile could be due to MMP-2-induced specific degradation of GelMA nanogels, in addition to the non-specific surface desorption and drug diffusion. As such, *in vitro* degradation profile of MNBM was determined by measuring their weight changes at each time point. As expected, the weight loss of electrospun membranes gradually increased with time; more importantly, the degradation rates were significantly accelerated when increasing the MMP-2 concentration in PBS (Fig. 3**J**). These results demonstrated that our proposed MNBM represented an enzyme-triggered on-demand drug delivery system, which could be specifically responsive to disease state.

3.4. In vitro cell viability, morphology, proliferation, and gene silencing

With our MNBM's physical characterization established, we then moved to evaluate their *in vitro* biological functions for tendon adhesion prevention. To ensure the intracellular delivery efficacy of the released siRNA complexes from the MNBM, leaching solutions of different membrane formulations were collected to incubate with NIH/3T3 fibroblasts for the following biological characterizations. First, we investigated the viability of NIH/3T3 cells via live/dead staining assay. As shown in Fig. 4**A and C**, there were mainly living cells in the control, PLLA and 10 %G2/PLLA groups, and almost no dead cells were found in these groups, indicating the excellent biocompatibility of our proposed delivery system.

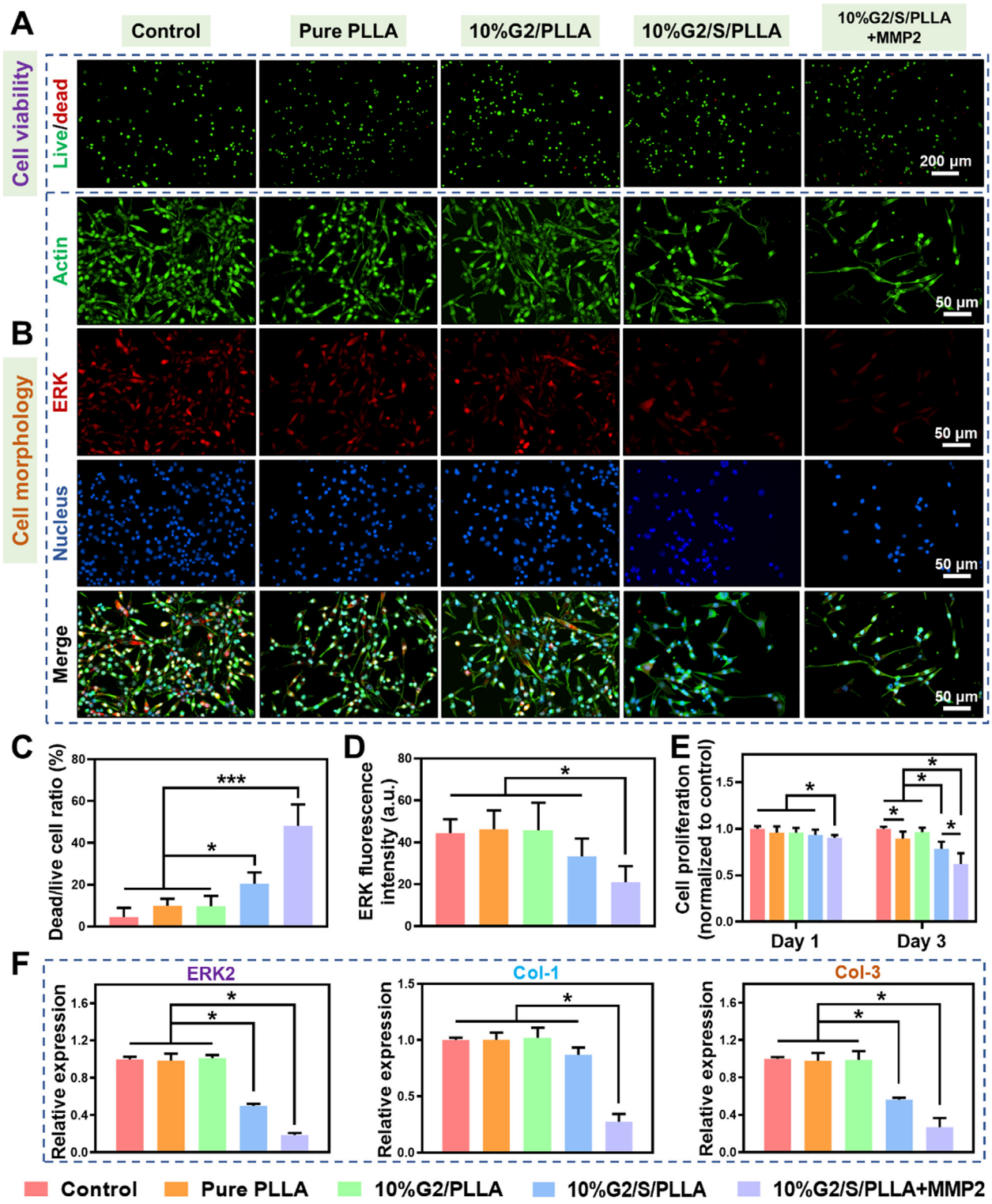

Fig. 4. *In vitro* biological evaluation of MNBM. (A) Live/dead staining and (C) corresponding dead/live cell ratio of NIH/3T3 fibroblasts treated with different membrane formulations for 3 days. Green fluorescence and red fluorescence indicated the viable and dead cells, respectively. (B) Immunofluorescence staining of ERK and F-actin. The green, red, and blue fluorescence represented the F-actin, cell nucleus, and ERK, respectively. (D) Corresponding semi-quantitative analysis of ERK expression in NIH/3T3. (E) Cell proliferation of NIH/3T3 after incubation with different membrane formulations for 1 and 3 days. (F) qRT-PCR analysis of mRNA expression levels of ERK2, and its downstream signaling factors including Col-1 and Col-3 in NIH/3T3 after culture with different membrane extracts for 3 days. Data were expressed as mean ± SD and evaluated by one-way ANOVA followed by Tukey's multiple comparison tests (n = 4, * represented $p < 0.05$, *** represented $p < 0.001$).

However, siRNA-containing groups exhibited obviously more cell death, and markedly higher dead/live cell ratio was observed in the MMP-2 treated groups (i.e., 10 %G2/PLLA + MMP-2). Subsequently, we performed the actin and ERK2 staining to observe the cell morphology and ERK2 protein expression. Our results revealed that NIH/3T3 cells were adhered onto the plate surface in the control, PLLA, and 10 %G2/PLLA groups, with cell spreading in an elongated and spindle shape (Fig. 4**B**). However, the number

of adhered cells was significantly lower in the siRNA-containing groups, and cells exhibited a decreased spreading area. Such phenomenon was more obvious in the MMP-2 treated group. Similarly, the ERK expression as indicated by the relative fluorescence intensity was remarkably lower in 10 %G2/S/PLLA + MMP-2 group, compared with other groups (Fig. 4**D**). Furthermore, the cell proliferation of NIH/3T3 cells after treatment with different material formulations was assessed by CCK-8. We found cell proliferation was prominently lower in the MMP2-treated siRNA-containing group after 1-day incubation as compared to other groups (Fig. 4**E**). After culture for 3 days, PLLA showed a slightly decreased cell proliferation rate than the control group, possibly due to the released toxic metabolites (e.g., lactic acid) by hydrolysis. Of note, significantly reduced cell proliferation was observed in the siRNA-containing groups, among which the MMP-2 treated group showed extremely lower proliferation. These findings suggested that MMP-2 could initiate siRNA release from the membrane scaffolds to suppress fibroblast growth, adhesion and proliferation.

To explore the underlying molecular mechanism, we further assessed the gene silencing efficacy of MNBM by examining the relative gene expressions of the targeted ERK2 and its downstream signaling molecules (Col-1 and Col-3) in NIH/3T3 fibroblasts using qRT-PCR. It was revealed that the ERK2 expression level was significantly downregulated in the siRNA-containing membrane groups (Fig. 4**F**). Notably, the addition of MMP-2 into 10 %G2/S/PLLA further decreased the ERK2 expression, as compared with 10 %G2/S/PLLA. Similar trends were also found in the relative gene expressions of Col-1 and Col-3 (Fig. 4**F**). These results were in accordance with those of above cell viability, adhesion and proliferation evaluation, indicating that the released siRNA from MNBM triggered by MMP-2 could preserve the bioactivity and induce the silencing effects of target genes. Such bioactivity maintenance may be partly due to the barrier effects of GelMA nanogels as a shell to protect the trapped siRNA from harsh external environment during electrospinning.

ERK2 has been demonstrated to be crucial in scar tissue formation by activation of local fibroblasts, improvement of fibroblast adhesion/proliferation, and over-secretion of collagen [15,16]. All these results demonstrated our MNBM could block the target gene expression efficiently through an MMP-2-triggered release of ERK2-siRNA, and consequently reduce fibroblast adhesion/proliferation and collagen deposition, showing great potential in attenuating peritendinous adhesion formation.

3.5. In vivo anti-tendon adhesion performance

To further explore the clinical relevance of our prepared MNBM under physiological conditions, we established a rat tendon injury model and covered the operation site with MNBM to prevent

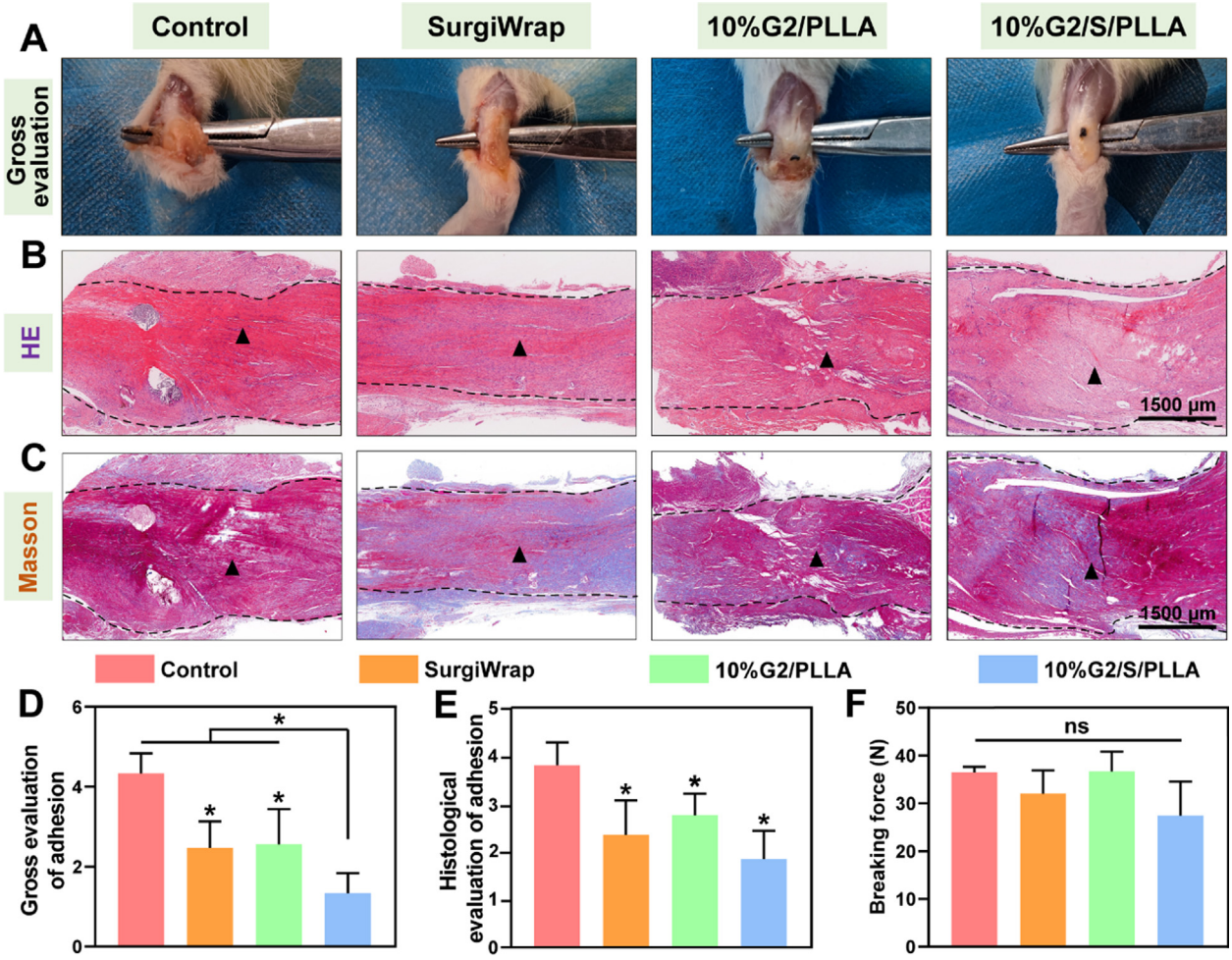

Fig. 5. *In vivo* anti-tendon adhesion therapeutic efficacy of MNBM. (A) Macroscopic observation and (D) corresponding semi-quantitative analysis of the peritendinous adhesion of surgical sites after implantation for 21 days. Histological evaluation of the harvested tissues by (B) H&E staining and (C) Masson staining. The black triangle indicated the repaired tendon tissue, while the dotted lines represented the boundary between the tendon and the peritendinous granulation tissue. (E) Histological assessment of the tendon adhesion based on H&E staining observation. (F) Maximal breaking forces of the repaired tendon. Data were expressed as mean ± SD and evaluated by one-way ANOVA followed by Tukey's multiple comparison tests (n = 4, * represented $p < 0.05$).

tendon adhesion to the surrounding tissues (**Fig. S3**). After surgery for 21 days, the surgical sites of the repaired tendons were directly observed, and the degree of adhesion was macroscopically assessed using a scoring system based on the surgical observation (Fig. 5**A and D**). We found no significant inflammation or ulcer around the incision area in all groups. In the control group, massive adhesion tissues were intertwined between the sutured tendon and surrounding tissue, which was difficult to separate using blunt instrument (corresponding to adhesion score of 4 to 5). In contrast, in the SurgiWrap and 10% G2/PLLA groups, only small bundles of fibrous tissues were observed at the site of repaired tendon, and it was feasible to separate them by blunt dissection (corresponding to adhesion score of 2 to 3). Importantly, the 10 %G2/S/PLLA group showed almost no dense adhesion tissue formation in the peritendinous area (corresponding to adhesion score of 1 to 2), revealing that MNBM release of siRNA during tendon healing process successfully reduced the peritendinous adhesion formation. The statistical results of adhesion scores for 10 %G2/S/PLLA group were the lowest among these four groups (Fig. 5**D**), further confirming its superior anti-adhesion capability.

We further assessed the peritendinous adhesion of the repaired sites by histochemical analysis including H&E staining and Masson's trichrome staining. As revealed in Fig. 5**B, C and E**, massive fibrous tissues were located between the repaired tendon and surrounding fibrosis tissue in the control group. These dense adhesion tissues grew into and merged with the intimal tendon, significantly reducing the tendon repair outcomes. However, there were loose fibrous bundles formed around the peritendinous area in the SurgiWrap and 10 %G2/PLLA groups. Notably, only little sporadic adhesion tissue was found in the 10 %G2/S/PLLA group, in which epitenon surface was relatively smoother as compared with other groups. It is well documented that, the tendon adhesion formation is often caused by excessive extrinsic healing in the reparative phase and remodelling phase, during which MMP-2 expression is elevated in the peritendinous area of repaired sites [10,34,35]. Therefore, these findings indicated our MNBM could act as a physical barrier to inhibit extrinsic fibroblast invasion while directing cell behaviours by MMP-2 responsive on-demand siRNA delivery to reduce collagen secretion, ultimately realizing adhesion-free tendon healing.

We also measured the maximum breaking force of the repaired tendon to investigate whether MNBM undermined the tendon healing process and reduced the repair quality. Our results revealed no significant difference in breaking force among these four groups (Fig. 5**E**). Such absence of detrimental effects on tendon healing might be owing to the porous structure of electrospun

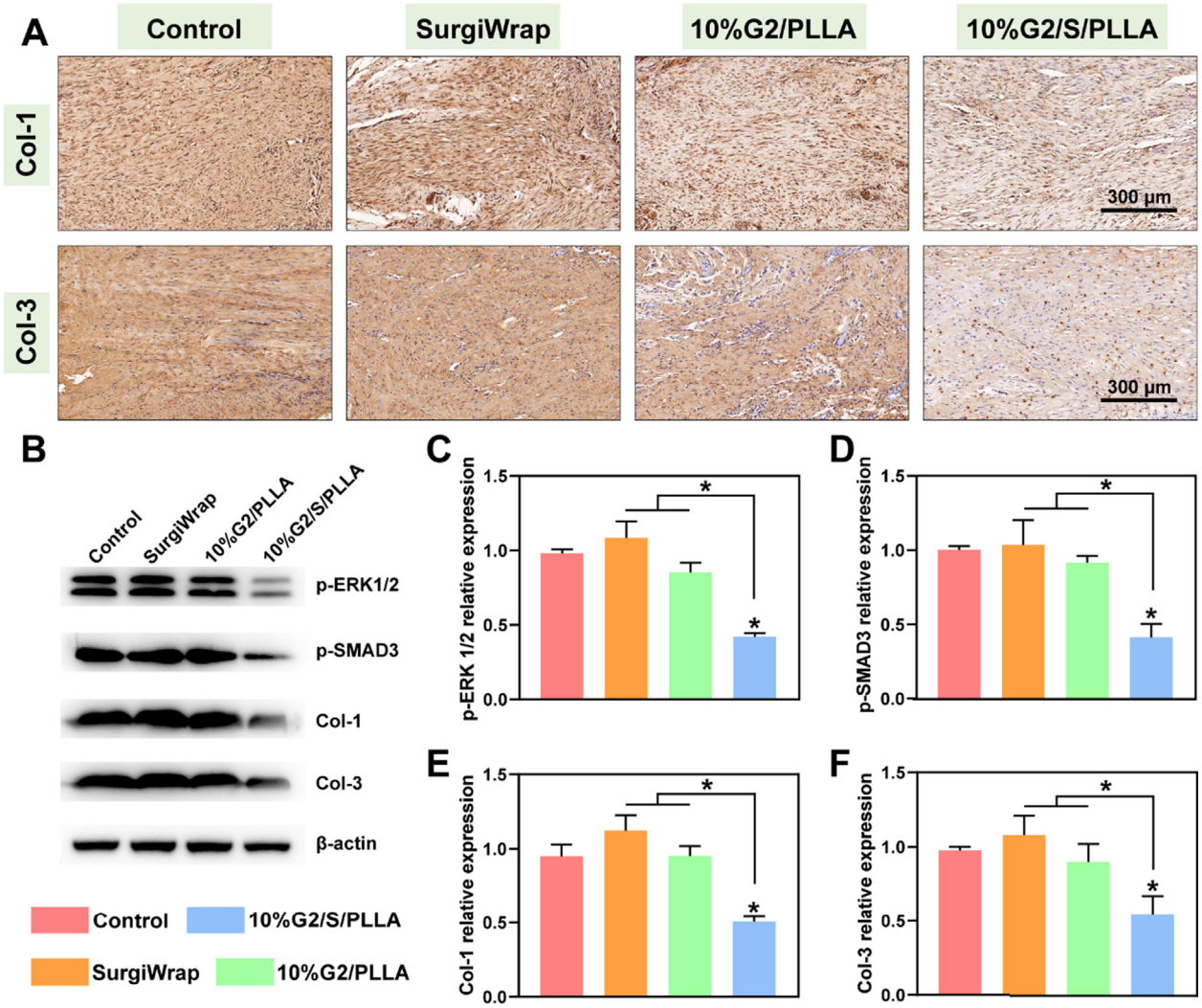

Fig. 6. Evaluation of target molecule expression in peritendinous adhesion tissues. (A) Representative images of immunohistochemical staining of Col-1 and Col-3. Western blot analysis of p-ERK1/2, p-SMAD3, Col-1 and Col-3 expressions. (B) The representative bands and the corresponding quantitative analysis of band intensity of (C) p-ERK1/2, (D) p-SMAD3, (E) Col-1, and (F) Col-3. Data were expressed as mean ± SD and evaluated by one-way ANOVA followed by Tukey's multiple comparison tests (n = 6, * represented $p < 0.05$).

fibrous membranes, which ensured nutrition/waste infiltration for intrinsic healing process.

To verify anti-adhesion mechanism of our MNBM, we further investigated the expression levels of target ERK2 and its downstream molecules like p-SMAD3, Col-1 and Col-3 [16,36]. We first performed immunohistochemical staining to analyze the expressions of downstream Col-1 and Col-3, which were the main components in the tendon adhesion tissue [37,38]. As displayed in the Fig. 6**A**, Col-1 and Col-3, indicated by yellow brown staining, appeared in all groups. Interestingly, weaker staining intensity of Col-1 and Col-3 in the peritendinous adhesion tissue was observed in 10 %G2/S/PLLA group, with their average optical density decreased by nearly 50%. This reinforced the statement that ERK2-siRNA released from MNBM could markedly reduce the downstream Col-1 and Col-3 expression, thereby suppressing the scar tissue formation. Next, we detected the protein expression of p-ERK1/2, p-SMAD3, Col-1, and Col-3 in the peritendinous adhesion tissue via western blotting, while using β-actin as the internal control (Fig. 6**B-F**). It was found that the 10 %G2/S/PLLA group showed significantly lower expression of p-ERK1/2, p-SMAD3, Col-1, and Col-3 among the four groups. These results were in line with those of *in vitro* qRT-PCR and ERK2 immunofluorescence staining assays, indicating the micro-environment-triggered ERK2-siRNA release during the healing process could downregulate the target gene expression, reduce collagen synthesis and contribute to the reduction of adhesion formation. Taken together, these data collectively demonstrated that our MNBM could serve as a promising platform for on-demand siRNA delivery to prevent adhesion formation, providing an appealing prospect for the clinical treatment of patients with tendon injuries.

4. Conclusion

In this study, we have successfully developed an intelligent fibrous membrane, MNBM, with enzyme-triggered on-demand ERK2-siRNA delivery capability for tendon adhesion prevention. Our MNBM could be prepared by first fabrication of siRNA-laden GelMA nanogels via nano-emulsification technique, and then co-electrospinning of these nanogels into PLLA fibers. In this system, GelMA nanogels offered a favorable nano-niche for siRNA retention. By changing the concentration of the precursor GelMA solution used for nano-emulsification, a nano-environment modulated siRNA release pattern could easily be realized. In addition, the resultant MNBM exhibited a micro-environment controlled siRNA delivery behavior, from which ERK2-siRNA could be triggered to release and downregulate the target gene expression in response to the MMP-2-elevated micro-environment during tendon repair. *In vitro* and *in vivo* results further demonstrated this micro- and nano-environment dual modulation strategy could effectively inhibit fibroblast growth/proliferation and reduce collagen production, attenuating peritendinous adhesion formation. Combined with other advantages like tailorable fiber structure, excellent swelling, degradation and mechanical performances, we believe our all-in-one MNBM will be a superior anti-adhesion barrier graft for tendon injury therapy. Compared with other electrospun fiber-based gene delivery systems for tendon adhesion prevention [6,14,39], our MTBM also has advantages including (1) simple and time-saving fabrication process; (2) off-the-shelf and tailorable nature to accelerate surgical operation; and (3) homogeneous and symmetric architecture to evade stress concentration and spatial separation between multi-layer components. Considering that overexpressed MMP was found in many other diseases like diabetes mellitus-associated skin impairment [40], osteoarthritis [41], tumor [42,43], we envision such intelligent drug delivery platform will find extensive applications in other tissue engineering fields.

CRediT authorship contribution statement

Qiang Zhang: Conceptualization, Methodology, Investigation, Writing – original draft. **Kui Ma:** Methodology, Investigation, Writing – original draft. **Chun-Hei Lam:** Methodology, Investigation. **Ho-Pan Bei:** . **Yu Liu:** Methodology, Investigation. **Xing Yang:** Supervision, Resources, Funding acquisition. **Xin Zhao:** Conceptualization, Supervision, Resources, Funding acquisition.

Declaration of Competing Interest

The authors declare that they have no known competing financial interests or personal relationships that could have appeared to influence the work reported in this paper.

Acknowledgements

The authors would like to thank Mr Hanbai Wu for assistance on the siRNA release experiments. This work was supported by the Health and Medical Research Fund from the Food and Health Bureau (FHB) of Hong Kong (Ref. No. 06173186), the Natural Science General Program of Jiangsu Science and Technology Department (BK20211083), Gusu Health Talent Training Program of Suzhou Health Commission (GSWS2020078), and Health Commission of Suzhou Municipality (SYS2019101).

Data availability statement

The data that support the findings of this study are available from the corresponding author upon reasonable request.

Appendix A. Supplementary data

Supplementary data to this article can be found online at https://doi.org/10.1016/j.matdes.2022.110737.

References

[1] Q. Zhang, Y. Yang, L. Yildirimer, T. Xu, X. Zhao, Advanced technology-driven therapeutic interventions for prevention of tendon adhesion: design, intrinsic and extrinsic factor considerations, Acta Biomater. 124 (2021) 15–32.
[2] S. Jiang, X. Zhao, S. Chen, G. Pan, J. Song, N. He, F. Li, W. Cui, C. Fan, Down-regulating ERK1/2 and SMAD2/3 phosphorylation by physical barrier of celecoxib-loaded electrospun fibrous membranes prevents tendon adhesions, Biomaterials 35 (37) (2014) 9920–9929.
[3] S. Liu, C. Hu, F. Li, X.J. Li, W. Cui, C. Fan, Prevention of peritendinous adhesions with electrospun ibuprofen-loaded poly (L-lactic acid)-polyethylene glycol fibrous membranes, Tissue Eng. Part A 19 (3–4) (2013) 529–537.
[4] X. Zhao, S. Jiang, S. Liu, S. Chen, Z.Y.W. Lin, G. Pan, F. He, F. Li, C. Fan, W. Cui, Optimization of intrinsic and extrinsic tendon healing through controllable water-soluble mitomycin-C release from electrospun fibers by mediating adhesion-related gene expression, Biomaterials 61 (2015) 61–74.
[5] O. Evrova, G.M. Bürgisser, C. Ebnöther, A. Adathala, M. Calcagni, E. Bachmann, J. G. Snedeker, C. Scalera, P. Giovanoli, V. Vogel, Elastic and surgeon friendly electrospun tubes delivering PDGF-BB positively impact tendon rupture healing in a rabbit Achilles tendon model, Biomaterials 232 (2020) 119722.
[6] S. Liu, F. Wu, S. Gu, T. Wu, S. Chen, S. Chen, C. Wang, G. Huang, T. Jin, W. Cui, Gene silencing via PDA/ERK2-siRNA-mediated electrospun fibers for peritendinous antiadhesion, Adv. Sci. 6 (2) (2019) 1801217.
[7] Y.L. Zhou, Q.Q. Yang, Y.Y. Yan, C. Zhu, L. Zhang, J.B. Tang, Localized delivery of miRNAs targets cyclooxygenases and reduces flexor tendon adhesions, Acta Biomater. 70 (2018) 237–248.
[8] E. Karousou, M. Ronga, D. Vigetti, A. Passi, N. Maffulli, Collagens, proteoglycans, MMP-2, MMP-9 and TIMPs in human achilles tendon rupture, Clin. Orthop. Relat. Res. 466 (7) (2008) 1577–1582.
[9] S.C. Juneja, E.M. Schwarz, R.J. O'Keefe, H.A. Awad, Cellular and molecular factors in flexor tendon repair and adhesions: a histological and gene expression analysis, Connect. Tissue Res. 54 (3) (2013) 218–226.
[10] A.E. Loiselle, G.A. Bragdon, J.A. Jacobson, S. Hasslund, Z.E. Cortes, E.M. Schwarz, D.J. Mitten, H.A. Awad, R.J. O'Keefe, Remodeling of murine intrasynovial tendon adhesions following injury: MMP and neotendon gene expression, J. Orthop. Res. 27 (6) (2009) 833–840.

[11] Y.M. Farhat, A.A. Al-Maliki, A. Easa, R.J. O'Keefe, E.M. Schwarz, H.A. Awad, TGF-β1 suppresses plasmin and MMP activity in flexor tendon cells via PAI-1: Implications for scarless flexor tendon repair, J. Cell. Physiol. 230 (2) (2015) 318–326.
[12] J.S. Ribeiro, E.A. Bordini, J.A. Ferreira, L. Mei, N. Dubey, J.C. Fenno, E. Piva, R.G. Lund, A. Schwendeman, M.C. Bottino, Injectable MMP-responsive nanotube-modified gelatin hydrogel for dental infection ablation, ACS Appl. Mater. Interfaces 12 (14) (2020) 16006–16017.
[13] K. Yue, G. Trujillo-de Santiago, M.M. Alvarez, A. Tamayol, N. Annabi, A. Khademhosseini, Synthesis, properties, and biomedical applications of gelatin methacryloyl (GelMA) hydrogels, Biomaterials 73 (2015) 254–271.
[14] C. Cai, X. Zhang, Y. Li, X. Liu, S. Wang, M. Lu, X. Yan, L. Deng, S. Liu, F. Wang, Self-healing Hydrogel Embodied with Macrophage-regulation and Responsive-gene-silencing Properties for Synergistic Prevention of Peritendinous Adhesion, Adv. Mater. 2106564 (2021).
[15] H. Ruan, S. Liu, F. Li, X. Li, C. Fan, Prevention of tendon adhesions by ERK2 small interfering RNAs, Int. J. Mol. Sci. 14 (2) (2013) 4361–4371.
[16] F. Li, C. Fan, T. Cheng, C. Jiang, B. Zeng, Efficient inhibition of fibroblast proliferation and collagen expression by ERK2 siRNAs, Biochem. Biophys. Res. Commun. 382 (2) (2009) 259–263.
[17] Y. Yang, T. Xu, Q. Zhang, Y. Piao, H.P. Bei, X. Zhao, Biomimetic, stiff, and adhesive periosteum with osteogenic–angiogenic coupling effect for bone regeneration, Small 17 (14) (2021) 2006598.
[18] X. Zhao, S. Liu, L. Yildirimer, H. Zhao, R. Ding, H. Wang, W. Cui, D. Weitz, Injectable stem cell-laden photocrosslinkable microspheres fabricated using microfluidics for rapid generation of osteogenic tissue constructs, Adv. Funct. Mater. 26 (17) (2016) 2809–2819.
[19] J. Kim, R. Gauvin, H.J. Yoon, J.-H. Kim, S.-M. Kwon, H.J. Park, S.H. Baek, J.M. Cha, H. Bae, Skin penetration-inducing gelatin methacryloyl nanogels for transdermal macromolecule delivery, Macromol. Res. 24 (12) (2016) 1115–1125.
[20] N. Kordalivand, D. Li, N. Beztsinna, J.S. Torano, E. Mastrobattista, C.F. van Nostrum, W.E. Hennink, T. Vermonden, Polyethyleneimine coated nanogels for the intracellular delivery of RNase A for cancer therapy, Chem. Eng. J. 340 (2018) 32–41.
[21] M. Chen, S. Gao, M. Dong, J. Song, C. Yang, K.A. Howard, J. Kjems, F. Besenbacher, Chitosan/siRNA nanoparticles encapsulated in PLGA nanofibers for siRNA delivery, ACS Nano 6 (6) (2012) 4835–4844.
[22] D. Cun, D.K. Jensen, M.J. Maltesen, M. Bunker, P. Whiteside, D. Scurr, C. Foged, H.M. Nielsen, High loading efficiency and sustained release of siRNA encapsulated in PLGA nanoparticles: quality by design optimization and characterization, Eur. J. Pharm. Biopharm. 77 (1) (2011) 26–35.
[23] P.-O. Rujitanaroj, Y.-C. Wang, J. Wang, S.Y. Chew, Nanofiber-mediated controlled release of siRNA complexes for long term gene-silencing applications, Biomaterials 32 (25) (2011) 5915–5923.
[24] Y. Yang, Q. Zhang, T. Xu, H. Zhang, M. Zhang, L. Lu, Y. Hao, J.H. Fuh, X. Zhao, Photocrosslinkable nanocomposite ink for printing strong, biodegradable and bioactive bone graft, Biomaterials 263 (2020) 120378.
[25] X. Lu, S. Shi, H. Li, E. Gerhard, Z. Lu, X. Tan, W. Li, K.M. Rahn, D. Xie, G. Xu, Magnesium oxide-crosslinked low-swelling citrate-based mussel-inspired tissue adhesives, Biomaterials 232 (2020) 119719.
[26] A. Plotnikov, K. Flores, G. Maik-Rachline, E. Zehorai, E. Kapri-Pardes, D.A. Berti, T. Hanoch, M.J. Besser, R. Seger, The nuclear translocation of ERK1/2 as an anticancer target, Nat. Commun. 6 (1) (2015) 1–11.
[27] S. Liu, M. Qin, C. Hu, F. Wu, W. Cui, T. Jin, C. Fan, Tendon healing and anti-adhesion properties of electrospun fibrous membranes containing bFGF loaded nanoparticles, Biomaterials 34 (19) (2013) 4690–4701.
[28] E. Güdemez, F. Ekşioğlu, P. Korkusuz, E. Aşan, İ. Gürsel, V. Hasırcı, Chondroitin sulfate–coated polyhydroxyethyl methacrylate membrane prevents adhesion in full-thickness tendon tears of rabbits, J. Hand Surg. 27 (2) (2002) 293–306.
[29] L. Li, X. Zheng, D. Fan, S. Yu, D. Wu, C. Fan, W. Cui, H. Ruan, Release of celecoxib from a bi-layer biomimetic tendon sheath to prevent tissue adhesion, Mater. Sci. Eng. C 61 (2016) 220–226.
[30] C. Hu, S. Liu, Y. Zhang, B. Li, H. Yang, C. Fan, W. Cui, Long-term drug release from electrospun fibers for in vivo inflammation prevention in the prevention of peritendinous adhesions, Acta Biomater. 9 (7) (2013) 7381–7388.
[31] L. Cheng, Y. Wang, G. Sun, S. Wen, L. Deng, H. Zhang, W. Cui, Hydration-enhanced lubricating electrospun nanofibrous membranes prevent tissue adhesion, Research 2020 (2020).
[32] Z. Guo, D. Bo, Y. He, X. Luo, H. Li, Degradation properties of chitosan microspheres/poly (L-lactic acid) composite in vitro and in vivo, Carbohydr. Polym. 193 (2018) 1–8.
[33] Y. Xu, Y. Gu, F. Cai, K. Xi, T. Xin, J. Tang, L. Wu, Z. Wang, F. Wang, L. Deng, Metabolism balance regulation via antagonist-functionalized injectable microsphere for nucleus pulposus regeneration, Adv. Funct. Mater. 30 (52) (2020) 2006333.
[34] A. Lomas, C. Ryan, A. Sorushanova, N. Shologu, A. Sideri, V. Tsioli, G. Fthenakis, A. Tzora, I. Skoufos, L.R. Quinlan, The past, present and future in scaffold-based tendon treatments, Adv. Drug Deliv. Rev. 84 (2015) 257–277.
[35] C.S. Klifto, J.T. Capo, A. Sapienza, S.S. Yang, N. Paksima, Flexor tendon injuries, J. Am. Acad. Orthop. Surg. 26 (2) (2018) e26–e35.
[36] T. Hayashida, M. de Caestecker, H.W. Schnaper, Cross-talk between ERK MAP kinase and Smad-signaling pathways enhances TGF-β dependent responses in human mesangial cells, FASEB J. 17 (11) (2003) 1–21.
[37] Y. Wang, L. Cheng, S. Wen, S. Zhou, Z. Wang, L. Deng, H.Q. Mao, W. Cui, H. Zhang, Ice-inspired superlubricated electrospun nanofibrous membrane for preventing tissue adhesion, Nano Lett. 20 (9) (2020) 6420–6428.
[38] J.E. Jackson, Z. Kopecki, P.J. Anderson, A.J. Cowin, Increasing the level of cytoskeletal protein Flightless I reduces adhesion formation in a murine digital flexor tendon model, J. Orthop. Surg. Res. 15 (1) (2020) 1–14.
[39] C. Cai, W. Wang, J. Liang, Y. Li, M. Lu, W. Cui, C. Fan, L. Deng, Y. Li, F. Wang, MMP-2 responsive unidirectional hydrogel-electrospun patch loading TGF-β1 siRNA polyplexes for peritendinous anti-adhesion, Adv. Funct. Mater. 31 (6) (2021) 2008364.
[40] A. Banerjee, V. Koul, J. Bhattacharyya, Fabrication of in situ layered hydrogel scaffold for the co-delivery of pgdf-bb/chlorhexidine to regulate proinflammatory cytokines, growth factors, and mmp-9 in a diabetic skin defect albino rat model, Biomacromolecules 22 (5) (2021) 1885–1900.
[41] H. Chen, Z. Qin, J. Zhao, Y. He, E. Ren, Y. Zhu, G. Liu, C. Mao, L. Zheng, Cartilage-targeting and dual MMP-13/pH responsive theranostic nanoprobes for osteoarthritis imaging and precision therapy, Biomaterials 225 (2019) 119520.
[42] M. Shu, J. Tang, L. Chen, Q. Zeng, C. Li, S. Xiao, Z. Jiang, J. Liu, Tumor microenvironment triple-responsive nanoparticles enable enhanced tumor penetration and synergetic chemo-photodynamic therapy, Biomaterials 268 (2021) 120574.
[43] J. Huang, Z. Xiao, Y. An, S. Han, W. Wu, Y. Wang, Y. Guo, X. Shuai, Nanodrug with dual-sensitivity to tumor microenvironment for immuno-sonodynamic anti-cancer therapy, Biomaterials 269 (2021) 120636.